Effect of surface intermixing on the morphology of Sb-terminated Ge(100) surfaces

L. H. Chan and E. I. Altman
Department of Chemical Engineering, Yale University, New Haven, Connecticut 06520
(Received 30 October 2000; published 19 April 2001)

The interaction of Sb with Ge(100) was investigated as a function of substrate temperature and Sb coverage using temperature programmed desorption, low energy electron diffraction, ion scattering, and scanning tunneling microscopy. An Sb desorption peak associated with multilayer physical adsorption was observed at 550 K while a second desorption peak at 980 K was attributed to Sb bound to the Ge surface. Four basic types of Sb clusters were identified at 320 K: a three-dimensional tetramer; a square, flat tetramer; dimers running perpendicular to the substrate dimer rows; and dimers running parallel to the dimer rows. The three-dimensional tetramer was observed to convert irreversibly to the flat tetramer, while the flat tetramer reversibly split to form the dimers. Diffusion of both the flat tetramers and the perpendicular dimers led to the formation of asymmetric (2×1) reconstructed islands. At 520 K, Sb started to displace Ge in the top layer creating pits at low Sb coverage. As the Sb coverage was increased, both islands and pits were observed. Intermixing between Sb and Ge was found in both the islands and the original surface layer. Intermixing, however, was limited between 520 K and 620 K when the Ge surface was covered with 1 monolayer or more of Sb, resulting in the smoothest Sb-terminated Ge surfaces. Regardless of how the Sb layer was prepared, annealing at 800 K roughened the surface severely and increased the amount of exposed Ge, even though no Sb desorbed at this temperature. The surface roughening was attributed to the increased surface area enabling Sb-Ge exchange without burying the lower surface tension Sb beneath the surface. Antimony is used as a surfactant to promote the growth of flat Ge films. The results demonstrate, however, that intermixing can lead to the surfactant severely roughening the surface if the growth of the surfactant layer is not carefully controlled.

DOI: 10.1103/PhysRevB.63.195309 PACS number(s): 68.55.Ac, 68.37.Ef, 68.35.Ct

I. INTRODUCTION

The observation that the addition of an adsorbate or surfactant can promote layer-by-layer or Frank–van der Merwe growth, or at least delay the onset of three-dimensional clustering in Stranski-Krastanov growth, has attracted considerable interest in recent years.[1–3] Although the mechanisms by which surfactants alter growth modes are still not clearly understood, experiments have revealed a number of similarities between systems where surfactants have been successfully used.[2,4–6] It has been shown that group V elements are very effective surfactants, even for such disparate systems as Ag(111) homoepitaxy and Ge growth on Si(100).[1,7–9] Other similarities include a greatly increased island density in the nucleation regime, which has been taken as an indication that the surfactant limits adatom diffusion rates.[4–7] More recently, it has been shown that the surfactant layer for Sb-mediated Ag homoepitaxy is an intermixed, ordered Sb-Ag alloy layer.[7–9] It has also been found that Sb and Ge tend to form intermixed surfaces, suggesting that surface intermixing may play a key role in surfactant-mediated thin film growth.[10,11] Therefore, we have systematically investigated the interaction of Sb with Ge(100) using temperature programmed desorption (TPD), low energy electron diffraction (LEED), ion scattering spectroscopy (ISS), and scanning tunneling microscopy (STM). The goals were to determine the conditions under which Sb and Ge intermix, the energy difference between an intermixed surface and an Sb adsorbate layer, and the effect of intermixing on the surface morphology.

The interaction of Sb with Si and Ge(100) has been studied using a number of techniques including x-ray and ultraviolet photoelectron spectroscopy,[10,12–15] surface x-ray diffraction,[16] LEED,[11,17,18] high energy electron diffraction,[10,12] STM,[17–24] scanning tunneling spectroscopy (STS),[20] ion channeling,[25] and x-ray absorption.[17] On Si(100), most studies agree that deposition of Sb multilayers followed by annealing at elevated temperatures to remove all but one Sb layer results in a (2×1) reconstructed surface. The Sb forms dimers, similar to the Si dimers seen on the bare (100) surface. At lower coverages and lower temperatures (below 820 K), however, there have been disagreements about whether Sb forms disordered three-dimensional clusters or dimers on the surface, and whether Sb displaces Si in the surface layer. In early STM work it was suggested that annealing an Si(100) surface with a low Sb coverage simply causes the Sb to aggregate into larger (2×1) reconstructed islands. Recently, however, Garni *et al.* provided convincing STM and STS evidence that at low Sb coverages annealing at 520 K causes Sb to incorporate into the Si surface creating ordered vacancies and (2×1) reconstructed Si islands on the surface.[20] It is unclear if intermixing also occurs when the Sb coverage approaches 1 monolayer (ML). At these coverages, it was found that the surface structure depends on preparation conditions. Based on STM images, it was suggested that depositing Sb at 650 K and annealing to 810 K results in Sb dimers on top of the Si surface. Increasing the annealing temperature to 970 K roughened the surface;[18] Garni *et al.* have suggested that the roughening is due to intermixing.[20] Prior work suggests that Sb behaves similarly on Ge(100). Annealing an Sb layer on Ge(100) also results in a (2×1) reconstructed surface with the $2\times$ direction perpendicular to that of the original Ge(100) terraces. Intermixing of Sb and Ge was first suggested by Rich *et al.*[10]

and later supported by the STM data of Falkenberg *et al.*[11]

The findings outlined above indicate that Sb can displace both Si and Ge atoms in the (100) surfaces, creating an intermixed surface. The kinetic pathway from initial Sb adsorption to incorporation into the surface layer and the impact of this intermixing process on the surface morphology, however, have not been addressed. Thus, the quest for a better understanding of the above processes motivated the current study of Sb adsorption on Ge(100) as a function of coverage and temperature. In this paper, it will be shown that when Ge(100) is exposed to Sb_4 at 320 K the Sb resides on top of the surface. At low Sb coverage, annealing to 520 K results in Sb-Ge exchange accompanied by pit formation. Despite the energetic preference for Sb incorporation into the surface, intermixing at 520 K can be precluded by depositing $\sim$1 ML Sb at lower temperatures. In this case, the lower Sb surface tension and the stronger Sb-Ge versus Sb-Sb interaction offset the energy gained by intermixing. Annealing to higher temperatures, however, results in surface roughening accompanied by intermixing. The roughening increases the surface area, allowing Sb-Ge exchange without burying Sb beneath either Sb or Ge. The results demonstrate how both coverage and temperature determine the structure of the surfactant layer. The implication of these results for surfactant-mediated thin film growth will be discussed.

II. EXPERIMENT

Experiments were performed using an UHV system equipped with a double-pass cylindrical mirror analyzer with angle resolving aperture for Auger electron spectroscopy (AES) and ion scattering spectroscopy, a quadrupole mass spectrometer, an ion gun for sputtering and ISS, LEED optics, and a high speed variable temperature scanning tunneling microscope. The base pressure of the system was maintained at 1×10^{-10} torr. The scanning tunneling microscope can operate in the temperature range of 300–900 K while recording STM movies at speeds exceeding 1 image/s.[26]

Germanium samples were cut from nominally undoped Ge wafers with a resistivity of 50–60 Ω cm; the wafers were oriented to within $\pm0.3°$ of (100). The samples were heated via conduction from a resistively heated Ta foil. The temperature was measured with a W-W/Re thermocouple housed within a 0.19 mm inner diameter Ta tube pressed against the face of the sample.[27] The sample was mounted so that no material other than Ta contacted the sample. Samples were cleaned by cycles of 500 eV Ar^+ sputtering at 550 K and annealing at 920 K until all contaminants were below the AES detection level and LEED yielded sharp (2×1) patterns. To obtain an atomically flat surface with large, evenly spaced terraces, a 30 nm Ge buffer layer was deposited at 630 K and then annealed at 920 K.[28]

A resistively heated Ta envelope containing Sb powder was used to evaporate Sb. Germanium was deposited from resistively heated W baskets containing melted Ge wafer fragments. A quartz crystal deposition rate meter was used to monitor and control the Ge deposition process. All STM images were acquired at room temperature.

Temperature programmed desorption was performed line of sight by placing the sample a few centimeters from the ionizer of the mass spectrometer. It is well known that gaseous Sb consists predominantly of polyatomic molecules, primarily Sb_4, when sublimed from the solid at temperatures up to 1450 K.[29] Because the mass of Sb_4 exceeds the 400 amu limit of the mass spectrometer, Sb, Sb_2, and Sb_3 were monitored during TPD experiments; all TPD curves are presented as the sum of the curves for the three species. A heating rate of 3 K/s was used.

A scattering angle of 130° and 1 keV He ions were used for ion scattering. To minimize the effect of sputtering on the results, low ion currents and short data acquisition times were used.

Electrochemically etched W tips were used for STM. Prior to use, the tips were cleaned by electron beam heating in UHV. Images were obtained at tunnel currents between 0.1 and 1.0 nA and sample biases between -3 and $+3$ V. Throughout this paper, sample biases are reported so that negative biases refer to occupied states and positive biases unoccupied states. Varying the tunnel current was not found to significantly affect the STM images.

III. RESULTS

A. TPD

Temperature programmed desorption was used to characterize the energetics of Sb adsorption on Ge(100). Figure 1(a) shows the thermal desorption curves as a function of Sb coverage for Sb deposited at 320 K. The results show that Sb binds to Ge(100) in at least three distinct states with the peak at 980 K filling first followed by the peaks at 550 and 1090 K. The high temperature peak at 980 K is attributed to Sb chemisorption. The position of this peak does not shift with increasing exposure. The peak at 550 K starts to appear slightly before the peak at 980 K saturates. The position of this peak shifts to higher temperature with increasing Sb exposure and does not saturate, typical of zero-order sublimation of a multilayer film. Therefore, this peak is assigned to Sb physisorption. The third peak, at 1090 K, was observed after prolonged Sb exposure as shown in Figure 1(b). This peak increases at a much slower rate than the multilayer peak at 550 K. Therefore, it was necessary to desorb all the physisorbed Sb before ramping the temperature to observe the peak at 1090 K. Otherwise, the mass spectrometer would saturate. The peak is also close to the melting point of Ge, and the temperature ramp had to be cut off at $\sim$1130 K. This peak did not shift with increasing exposure, nor did it saturate. In addition, the 1090 K peak became more intense when TPD experiments were performed repeatedly with the heating ramp stopped at 980 K. A possible explanation for these results is that the peak is due to Sb incorporation into the bulk followed by surface segregation and rapid desorption at high temperatures. The phase diagram is consistent with this picture. The solubility of Sb in Ge is roughly 0.035 at. % at 1070 K and falls as the temperature increases toward the melting point.[30]

As shown in Fig. 1(c), the ratio of Sb_2+Sb_3 to $Sb+Sb_2+Sb_3$ for the chemisorption peak increases with increasing Sb exposure. At saturation, the ratio is indistinguishable

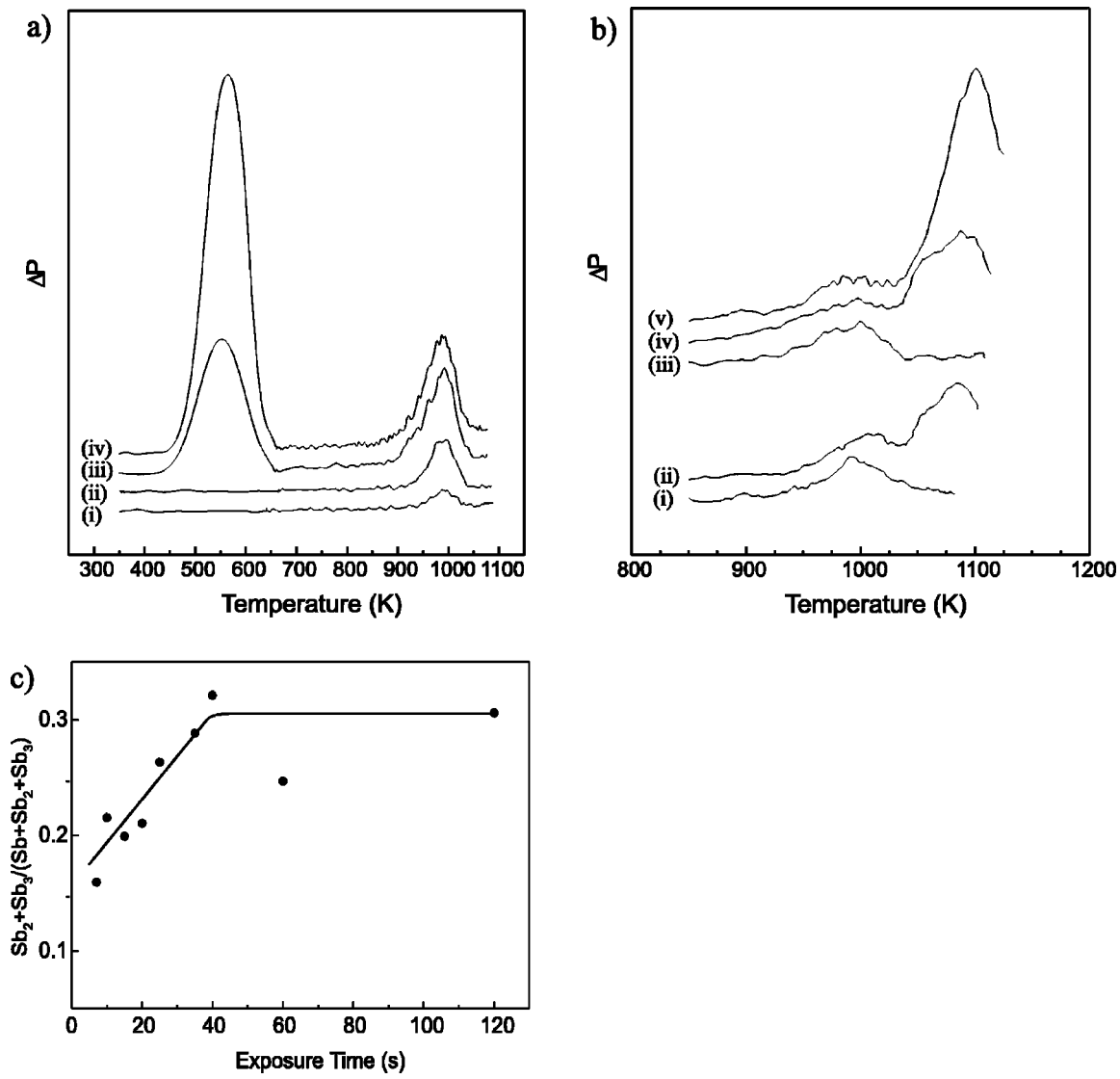

FIG. 1. (a,b) Series of TPD curves for Sb desorption from Ge(100). (a) Sb was deposited at 320 K for (i) 5 s, (ii) 20 s, (iii) 65 s, and (iv) 80 s. (b) The Ge(100) sample was annealed to 620 K for 60 s after depositing Sb for (i) 60 s and (ii) 600 s at 320 K and (iii) 60 s, (iv) 1220 s, and (v) 1800 s at 650 K. The curves in (a) and (b) are taken as the sum of the Sb, Sb_2, and Sb_3 desorption signals; the fraction of the signal due to the polyatomic species is plotted as a function of exposure time for the peak at 980 K in (c).

from that for Sb multilayers that are known to sublime as Sb_4. Therefore, this suggests that the desorbing species changes from Sb and Sb_2 to Sb_4 as the coverage increases. At temperatures above 955 K, the (2×1) reconstruction of the Ge(100) surface is lifted as the mobility of the surface atoms increases.[31] Therefore, the Ge and Sb atoms on the surface no longer exist as dimers but rather as individual atoms. At low coverages and high temperatures, the Sb is likely to be distributed across the surface and thus the distance between the Sb atoms can be large. As a result, the Sb tends to desorb as monomers. As the coverage increases, the probability of finding an adjacent Sb increases leading to an increase in the desorption signal due to Sb_2 and Sb_4. Despite the changes in the nature of the desorbing species, no other differences were observed between the Sb, Sb_2, and Sb_3 desorption traces. These results indicate that the desorption rate is limited by breaking the Sb-Ge bonds rather than reforming the tetramer. This is not surprising given the large temperature difference between the single and multilayer desorption peaks.

The much stronger interaction between Sb and Ge versus Sb and Sb, as well as the lower Sb surface tension, indicates that all the Sb must lie on the topmost layer at temperatures above the Sb sublimation temperature. This has important implications for intermixing and the surface morphology. Since intermixing requires Sb replace Ge in the surface, as long as the surface area is constant, intermixing cannot occur beyond a maximum Sb coverage. Increasing the coverage beyond this maximum would dictate either burying Sb beneath Sb, which would lead to rapid sublimation of the second layer Sb, or Sb beneath Ge, which is not favored because of the higher Ge surface tension. This suggests that the surface structure should depend strongly on Sb coverage and deposition or annealing temperature, with low coverages and

high temperatures favoring intermixing while high coverages and low temperatures should prevent intermixing. Therefore, to investigate energy differences between intermixed Sb and Sb on top of the Ge surface, we varied the Sb deposition temperature and studied the effect of annealing. Figure 1(b) compares Sb desorption for Sb deposited at 320 K and annealed above 620 K versus Sb deposited at 620 K, both for exposures corresponding to more than 1 ML (1 ML = 1 adatom/substrate atom = 6.3×10^{14} atoms/cm^2). The curves show only the chemisorption peak and are identical. In addition, Fig. 1(b) reveals no significant coverage dependence for the chemisorption peak, and no effect was observed on the chemisorption peak due to annealing, independent of the initial Sb coverage. Thus the TPD results suggest that either the energy difference between on-top and intermixed Sb is very small, or the surface structure is independent of the Sb coverage and temperature. In Sec. III D, it will be shown that below 800 K the surface structure does depend strongly on Sb coverage and temperature. The surface, however, can rapidly roughen to increase the surface area and allow intermixing at high desorption temperatures and high Sb coverages. Thus the TPD curves reflect an intermixed surface, regardless of the initial Sb coverage.

B. LEED

Low energy electron diffraction was used to characterize the order of the Sb-covered Ge(100) surface as a function of annealing temperature; the results are summarized in Fig. 2. The clean Ge(100) surface prepared by depositing a Ge buffer layer and annealing shows the expected sharp, two-domain (2×1) pattern with low background as shown in Figs. 2(a) and 2(b). As Sb was deposited on the surface at 320 K, the half-order spots became much weaker while the intensity of the integer-order spots remained roughly constant up to 1 ML. As shown in Figs. 2(c) and 2(d) for a coverage of roughly 1 ML, at low energies the half-order spots are completely obscured while at higher energies faint half-order spots streaking along [0,1] and [1,0] could be detected. Annealing the surface at either 520 K, as shown in Figs. 2(e) and 2(f), or 620 K did not change the LEED pattern. Figures 2(g) and 2(h) show that after annealing to 800 K the streaking decreases and the half-order spots are completely recovered, resulting in a pattern similar to the clean surface. This change is not due to Sb desorption since 800 K is well below the monolayer desorption peak as shown previously in TPD [Fig. 1(a)], or bulk diffusion since no change in the Sb AES peaks (not shown here) were observed after annealing. Increasing the Sb exposure beyond 1 ML at 320 K caused the integer-order spots to weaken; however, after annealing to 620 K to remove physisorbed Sb, the LEED patterns were indistinguishable from those shown in Figs. 2(e) and 2(f). In Sec. III D it will be shown that the Sb is dimerized under all the conditions described above and that the changes in the LEED patterns can be attributed to changes in the size and morphology of the (2×1) domains.

C. ISS

The monolayer sensitivity of ISS was exploited to characterize the composition of the surface layer of Sb-covered

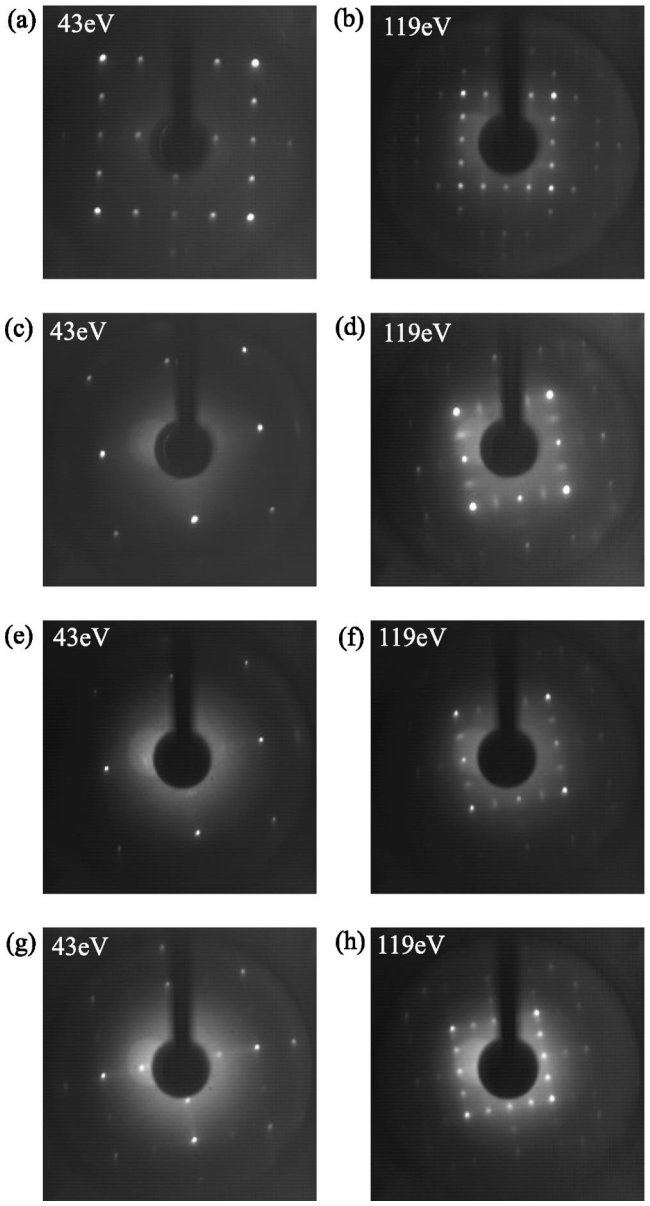

FIG. 2. Low energy electron diffraction patterns for clean Ge(100) (a,b), and Ge(100) covered by 1 ML of Sb after deposition at 320 K (c,d), after annealing at 520 K (e,f), and after annealing at 800 K (g,h).

Ge(100) as a function of temperature. Figure 3 shows the energy spectra for He scattering from clean and Sb-covered Ge. For the clean Ge(100) surface, Fig. 3(a), a single peak at $E/E_0=0.83$ was observed as expected for He scattering at 130° from nuclei with masses of 73 amu. After depositing 3 ML of Sb near 320 K, the Ge peak disappeared leaving only the higher energy peak associated with the heavier Sb, as shown in Fig. 3(b). Annealing at 620 K desorbs all physisorbed Sb according to TPD. Following this treatment, the AES signal (not shown here) decreased dramatically, to a level consistent with saturation of the TPD peak associated with chemisorption. Figure 3(c), however, shows a much smaller change in ISS: the appearance of a shoulder at lower energy. While further annealing to 800 K results in no per-

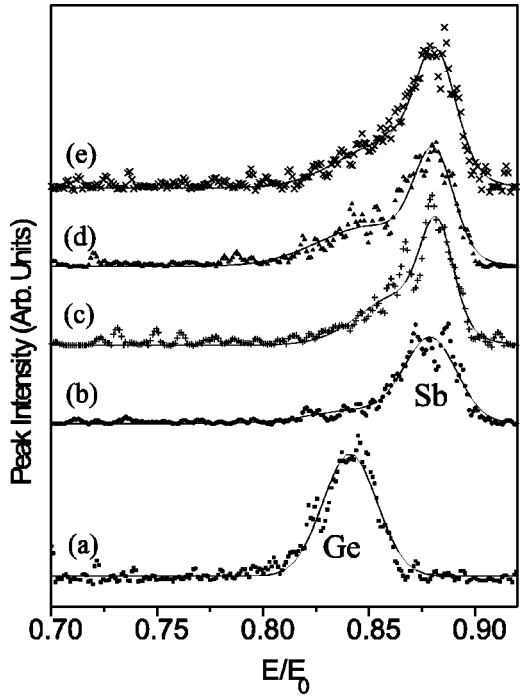

FIG. 3. Ion scattering spectra for (a) clean Ge(100), (b) 3 ML of Sb deposited at 320 K, (c) 3 ML of Sb deposited at 320 K and annealed at 620 K, (d) 3 ML of Sb deposited at 320 K and annealed at 800 K, and (e) 3 ML of Sb deposited at 620 K.

ceptible difference in AES spectra, the ISS spectrum in Fig. 3(d) shows that the low energy shoulder increases in intensity relative to the Sb peak and it is now clear that the energy of the shoulder corresponds to Ge at $E/E_0=0.83$. Thus, even though 800 K is well below the desorption peak for chemisorbed Sb, annealing to this temperature exposes the Ge substrate. Deposition at 620 K for an equivalent exposure of Sb, 3 ML, yields a similar ISS spectrum as 320 K deposition followed by 620 K annealing as shown in Fig. 3(e).

D. STM

1. Antimony adsorption at 320 K

Since Sb and Ge may exchange places following Sb deposition onto Ge, it is necessary to develop a capability to distinguish Sb from Ge in STM images. Therefore, we studied Sb_4 adsorption at 320 K where prior studies on Si(100) indicate that all the Sb stays on top of the surface, thus enabling definitive characterization of Ge and Sb.

Figure 4 shows the results for 0.07 ML of Sb. The coverage is determined by counting the density of the features in wider range STM images. The images reveal four basic types of Sb clusters. Following Mo's work on Sb on Si(100),[21–24] type *A* is identified as a ball-shaped Sb tetramer. Although its structure is not resolvable by STM, Mo has suggested that it resembles the three-dimensional tetrahedral Sb_4 molecules found in the gas phase. In the type *B* clusters, four lobes can be seen and they are identified as square, flat tetramers. Type *B* clusters reside either centered on top of the Ge dimer row or half on-top and half over the trough as shown in Fig. 4(d). Type *C* clusters are Sb dimers with the dimer bond perpendicular to the Ge dimers on the terrace. Type *C* dimers are always found directly on top of the Ge dimer rows. Type *D* clusters are dimers with the dimer bond parallel to the Ge dimers on the terrace. It should be noted that it can be argued that the type *B* clusters are simply pairs of type *C* or *D* dimers rather than a tetramer. The *B* clusters, however, appear distinctly different from either Sb or nonbuckled Ge dimers in the same image. Unlike the dimers, the individual atoms are resolved and the *B* clusters appear to have fourfold rather than twofold symmetry. In addition, the *B* clusters can diffuse on the surface as a single unit as described later in this paper.

The sequence of images in Fig. 4 also shows that the different types of cluster can interconvert and diffuse at room temperature. In the 70 s between recording the images in Figs. 4(a) and 4(b), the type *A* cluster converted into a type *B*

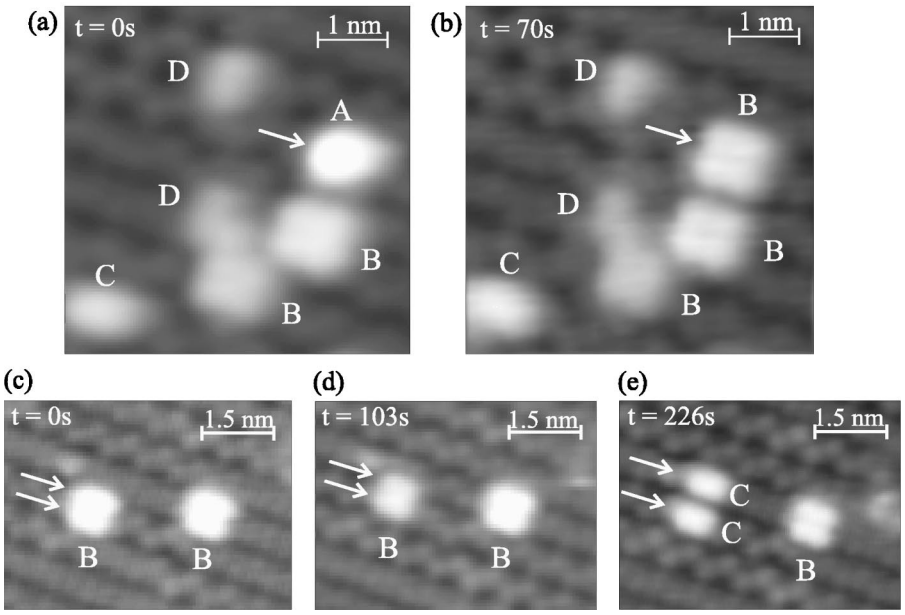

FIG. 4. Scanning tunneling micrographs obtained after depositing 0.07 ML Sb at 320 K. All images were acquired with $V_s=-1.25$ V and $I_t=0.5$ nA. Four distinct types of Sb cluster are labeled *A*, *B*, *C*, *D* in (a); after 70 s the *A* type cluster converts to a *B* type cluster (b). Images (c) and (d) recorded 103 s apart show a *B* cluster hopping one lattice constant; 123 s later, the *B* cluster has dissociated into two *C* clusters.

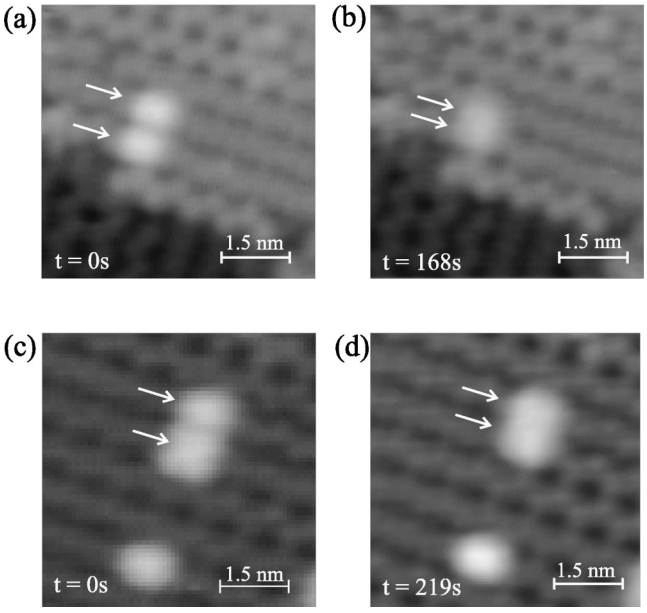

FIG. 5. Sequences of STM images showing two *C* type dimers (a) recombining to form a *B* type flat tetramer (b) and a flat tetramer and a *C* type dimer (c) combining to form a string composed of three pairs of Sb dimers (d). All images were acquired with $V_s = -1.25$ V and $I_t = 0.5$ nA.

cluster. The four lobes in the newly formed *B* cluster confirm the assignment of the type *A* cluster to a three-dimensional Sb tetramer. No conversions of type *B* clusters back to *A* clusters were observed, suggesting that the conversion from *A* to *B* is irreversible. The type *B* clusters were observed to diffuse and to split into two type *C* clusters. Comparing Figs. 4(c) and 4(d) shows that the *B* cluster at the left of the image has shifted one lattice constant, going from being centered directly on top of a Ge dimer row to half of the tetramer lying over the trough. This indicates that diffusion of intact *B* clusters perpendicular to the substrate dimer row direction occurs by hopping half the distance of the surface unit cell. Of 159 type *B* clusters imaged, 50 were in the on-top position. If it is assumed that the *B* clusters are sufficiently mobile to establish an equilibrium site distribution, then these numbers suggest that the on-top position is 0.020 eV higher in energy[32] than having half the tetramer over the trough. Conversion of *B* type clusters into two type *C* dimers was also observed, as shown in Figs. 4(d) and 4(e). This conversion was reversible, as shown in Figs. 5(a) and 5(b) which show two type *C* dimers coming together to form a type *B* square, flat tetramer. The splitting and reforming of the type *B* tetramers provides a second pathway for tetramer diffusion perpendicular to the Ge dimer rows.

Type *B* and *C* clusters are the basic building blocks for strings of Sb dimers that were observed at higher Sb coverages. This formation of Sb strings was also observed with STM as shown in the images in Figs. 5(c) and 5(d) which show a *B* type on-top tetramer moving to an in-trough position to join a dimer, thus forming a string composed of three pairs of Sb dimers.

Of the four types of Sb clusters described above, types *A*, *C*, and *D* have been observed on Si(100).[21–24] The population distributions for types *A* through *D* are 14%, 55%, 30%, and 1%, respectively; these statistics are based on categorizing over 300 Sb clusters. The low density of type *A* tetramers and their irreversible conversion to type *B* tetramers suggest that type *B* is lower in energy. There is a barrier, however, to converting the three-dimensional tetrahedral structure of the gas phase molecule into the square, flat structure that is favored on the surface. The conversion from type *B* to type *C* is reversible. If the type *B* and *C* populations are in equilibrium at 300 K, then the energy difference between these two states is roughly 0.108 eV. The low population of the type *D* parallel dimers suggests that these are higher in energy than either the *B* or *C* clusters. This is not surprising since parallel dimers are expected to be energetically unfavorable because this arrangement requires dimer bonds along the same direction in adjacent layers while the perpendicular direction is the epitaxial direction.

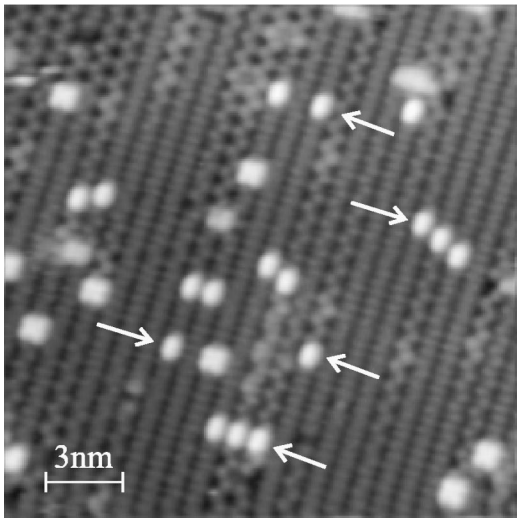

FIG. 6. Image of an area that was not scanned previously showing flat tetramers and paired and unpaired dimers. The surface was prepared by depositing 0.07 ML of Sb at 320 K. $V_s = -1.25$ V and $I_t = 0.5$ nA.

In prior work on Sb on Si(100) it was found that the STM tip could convert Sb precursor states into pairs of dimers, particularly at high biases.[21–24] For Sb on Ge(100), however, there was no evidence that the tip induced the changes shown in Figs. 4 and 5. The image in Fig. 4(c) shows two type *B* tetramers that were subjected to the same tunneling conditions while being imaged. The same area was scanned for over 10 min at biases ranging from -3 to 2 V, yet one tetramer remained intact, suggesting that the dissociation of the other tetramer was not induced by the tip. In addition, we imaged numerous type *A* tetramers at varying biases and saw no correlation between the tip bias and the conversion to type *B* tetramers. Finally, the changes we observed were much slower than the imaging rate, and so many images could be collected without any changes observed between images. Therefore, the first image collected of a new area likely reflects the appearance of the surface prior to any possible tip-induced conversion or diffusion; such an image is shown in Fig. 6. It shows pairs of dimers residing at adjacent rows as well as dimers that are not paired. Since at least 99%

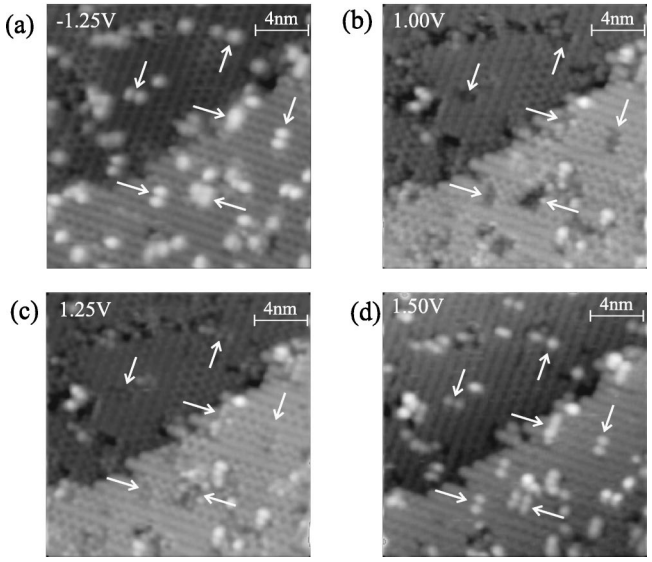

FIG. 7. Scanning tunneling micrographs of the same area obtained while imaging filled (a) and empty states (b)–(d). The arrows highlight the locations of the Sb clusters. The surface contained 0.07 ML Sb that was deposited at 320 K. The Sb clusters have lower apparent height in empty state STM images at low positive sample biases.

of the Sb arrives on the surface as Sb_4, unpaired dimers would have to be due to tetramers that split, followed by diffusion. Thus, tip-induced diffusion can be eliminated as the source of the observed structures.

Because the tunneling current depends on the local density of states integrated between the Fermi level and the imaging bias, chemically different species can frequently be distinguished by comparing STM images obtained at different biases.[33,34] Figure 7 shows how the appearance of Sb deposited onto Ge(100) at 320 K (where Sb resides on top of the Ge surface) changes as the bias is varied from -1.25 to $+1.5$ V. In the filled state images, the apparent height of the Sb clusters ranges from 0.14 to 0.27 nm. In contrast, the Sb clusters are not visible in unoccupied state images simultaneously acquired at 1 V. As the bias was increased, the apparent height of the Sb clusters increased and by 1.5 V the unoccupied state image was indistinguishable from the occupied state image. Similar behavior has been observed for H on Si(100).[35] Although the magnitude of the apparent height difference between Sb clusters in filled and empty state images was tip dependent, at 1 V the Sb clusters consistently appeared significantly lower than both the Ge(100) step height and the cluster height in filled state images. Thus, imaging in the range where tunneling into the unoccupied states of Ge is dominant can be used as a guide to distinguish Sb from Ge at elevated temperatures where intermixing may occur.

The results described above all focus on low coverages where the Sb atoms appear as isolated small clusters. At higher Sb coverages near room temperature, the Sb tended to form strings of dimers oriented perpendicular to the dimer rows of the Ge substrate as shown in the STM images in Fig. 8. The images show that the strings are interrupted by frequent antiphase domain boundaries, which is not surprising given the observed limited mobility of the Sb dimers and tetramers at these low temperatures. The images also show that the (2×1) domains are considerably longer along the dimer rows, the $1\times$ direction, than perpendicular to the rows, the $2\times$ direction. This difference in surface order along the two directions can explain the much greater attenuation of the half-order spots versus the integral-order spots in LEED patterns obtained at these coverages. All the integer-order spots are enhanced because the dimer directions alternate across monatomic steps, leading to equal populations of (1×2) and (2×1) domains.

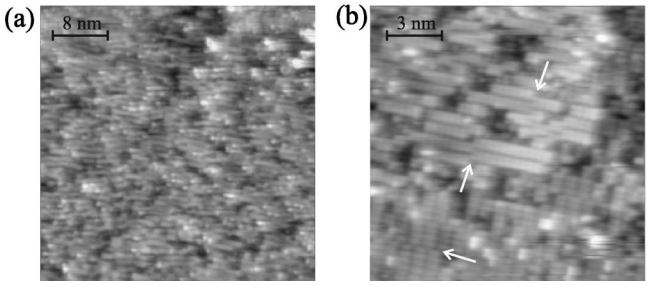

FIG. 8. Images (a) and (b) of 0.8 ML Sb deposited at 320 K. Strings of Sb dimers were formed with many antiphase domain boundaries indicated by the arrows in the smaller scale image (b). The sample biases were (a) -1.00 V and (b) -1.25 V.

Figure 8 also reveals only symmetric Sb dimers. In contrast, the images in Figs. 4–6 show both symmetric and asymmetric dimers in the Ge substrate. These results are typical, with STM images of the clean Ge(100) surface showing alternating domains of symmetric and asymmetric dimers.[36] While the buckling of Sb dimers on Ge(100) has been debated in the literature, even if the Sb dimers buckle the asymmetry will be difficult to detect with STM; the papers that support buckled Sb dimers suggest a dimer tilt of only 1° compared to 20° for Ge.[16,37–39] Thus, the asymmetry of the dimers can also be used to differentiate Sb from Ge.

2. Effect of annealing on Sb layers on Ge(100)

The morphology of Sb-covered Ge(100) surfaces was found to depend strongly on annealing temperature. Annealing below 520 K simply improved the ordering of the surface. At low coverages, the Sb changed from the randomly distributed clusters shown in Sec. III D 1 to strings of dimers. Annealing low Sb coverages at or above 520 K created pits on the surface as shown in Fig. 9. Figures 9(a) and 9(b) show the surface with 0.07 ML Sb deposited at 320 K before and after annealing; the coverage was determined by the density of Sb clusters in STM images prior to annealing. The disappearance of the Sb clusters after annealing was not due to either Sb desorption or bulk dissolution. The TPD experiments show that no submonolayer Sb is desorbed at temperatures lower than $\sim$870 K. In addition, Auger spectra taken after annealing showed no decrease in the Sb peak intensity, confirming that all the Sb must remain on the outermost layers. A few large islands composed of 100–300 dimers were occasionally observed on terraces wider than about 80 nm; one such island can be seen in Fig. 9(b). These islands

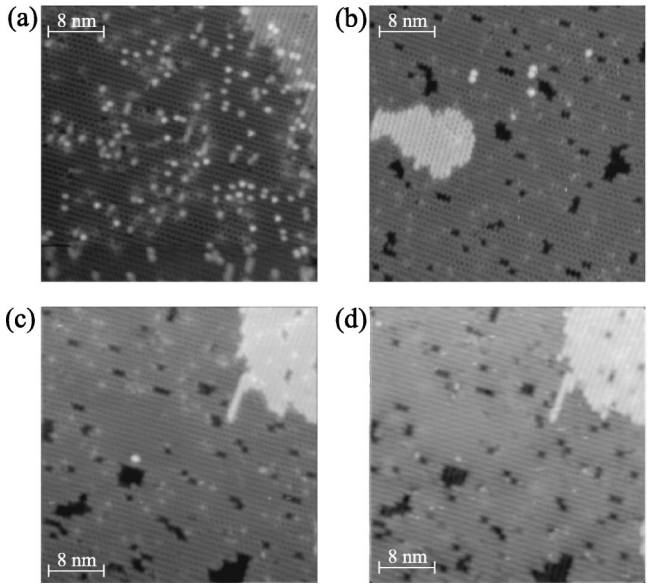

FIG. 9. Images of 0.07 ML of Sb deposited at 320 K (a) and then annealed at 520 K (b)–(d). The Sb clusters that were originally on top of the Ge substrate (a) disappeared after annealing at 520 K (b) leaving pits and a low density of islands on the surface. Filled state (c), −1.25 V, and empty state (d), 1.00 V, images of the same area showing step roughening caused by the displaced Ge.

consisted mainly of Ge dimers since they exhibited the Ge(100) step height in both filled and empty state STM images. Figure 9(b) also shows buckled dimers in the island, another indication that the islands contain Ge. After annealing at 520 K, there were also noticeable changes around step edges as shown in Fig. 9(c) The step edges appear roughened with strings of dimers. These dimers exhibited the same height in both filled and empty state STM images, as shown in Figs. 9(c) and 9(d), implying that they are Ge dimers. Since no Sb is desorbed from the surface at 520 K, it is assumed that Sb incorporates into the top layer and/or attaches to existing steps; the Sb incorporation is accompanied by pitting. The displaced Ge atoms diffuse on the surface, and either nucleate islands or attach to existing steps, thus roughening the steps. Because of the very low Sb coverage, it was difficult to definitively identify Sb clusters embedded in the Ge substrate from bias dependent imaging. Displacive incorporation has previously been reported for As and Ge on Si(100).[40]

When the Sb coverage was increased above 0.1 ML, annealing at 520 K created many small islands and pits. Figures 10(a) and 10(b) show a surface with 0.4 ML of Sb deposited at 320 K before and after annealing to 520 K. After annealing, the island and pit coverages are 0.32 ML and 0.05 ML, respectively. Simultaneously acquired filled and empty state images of the annealed surface are shown in Figs. 10(c) and 10(d). While all the dimers in a layer have the same apparent height in the filled state image [Figure 10(c)], segments of the dimer rows appear dim in the empty state image as indicated by the arrows in Fig. 10(d). The appearance of buckled dimers in the islands, and the contrast difference between dimers in the islands indicate that they are composed of both Sb and Ge. Increasing the annealing temperature to 620 K

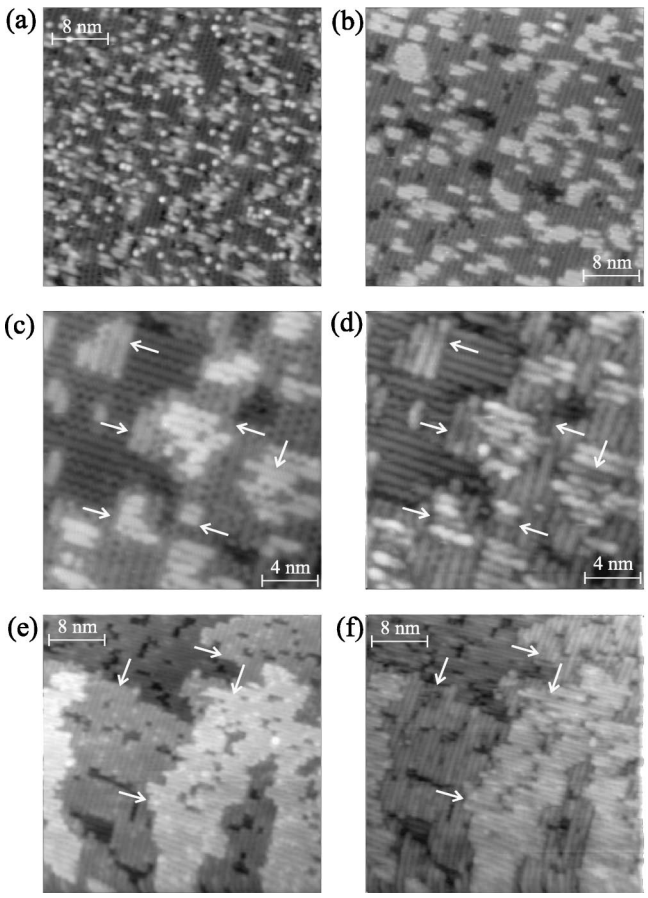

FIG. 10. Scanning tunneling micrographs of 0.4 ML of Sb deposited at 320 K before (a) and after (b)–(d) annealing at 520 K. $V_s = -1.25$ V for (a) and (b). Filled state (c), −1.50 V, and empty state (d), 1.00 V, images of the same area show contrast between dimers on the same level in the empty state image but not in the filled state. After annealing at 620 K, the filled state (e), −1.25 V, and empty state (f), 0.80 V, images show island coalescence and contrast variations between the dimers on all exposed levels in the empty state image. The arrows highlight segments of the dimer rows that appear dimmer in the empty state images.

results in coalescence and attachment of the islands to the steps as shown in Fig. 10(e). The original substrate layer is now characterized by narrow pits running perpendicular to the dimer rows, while wider, more symmetric pits are observed on the ad-islands. Again, the dimers in each layer all appear at the same height in the filled state image in Fig. 10(e), while the empty state image in Fig. 10(f) shows that some dimers appear lower than others. These dim dimers are observed on all three layers, indicating that all the exposed layers are intermixed.

Intermixing of the islands at 0.4 ML can be understood as follows. Antimony dimers diffuse until they exchange places with substrate Ge dimers. The displaced Ge dimers diffuse across the surface until they collide with other Ge dimers and nucleate an island. Unlike the situation at very low coverages, at the start of the process the Sb coverage on the terraces is still significant and so the remaining diffusing Sb dimers can attach to Ge islands. Addition of Ge to the islands leaves the Sb in the same environment as if the Sb ex-

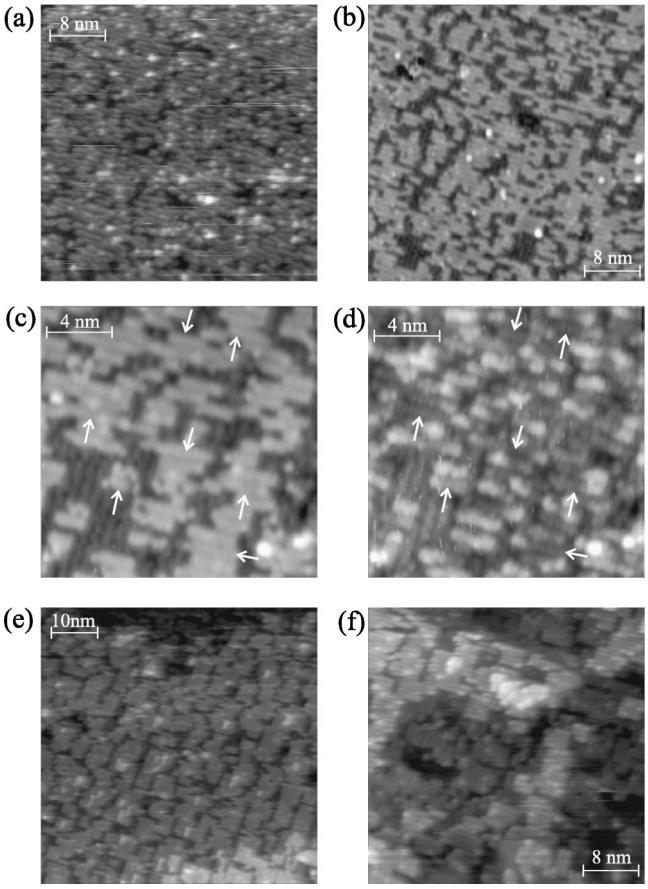

FIG. 11. Images of 0.8 ML of Sb deposited at 320 K before (a) and after annealing at (b)–(d) 520 K, (e) 620 K, and (f) 800 K. Comparison of the filled state (c) and empty state (d) images of the same area shows that most of the islands appear darker in the empty state image as highlighted by the arrows that point to the same location in the two images. Annealing at higher temperatures (e) and (f) results in roughening with multiple layers exposed. All images were obtained with $V_s = -1.25$ V except (c) (1.00 V).

changed with Ge in the terraces.

The intermixing in the pits can proceed through the same mechanism as on the original terraces. That is, as the pits become large, the influence of the surrounding step edges decreases and the terrace at the bottom of the pit begins to become indistinguishable from the original terraces. Thus a driving force for incorporation into the pits develops, and the probability of diffusing Sb incorporating into the pits prior to attaching to the step edges increases.

After 0.8 ML of Sb were deposited at 320 K, short strings of Sb dimers along with some second layer Sb was observed as shown in Fig. 11(a). After annealing at 520 K, the ad-dimers arranged in a serpentine pattern and became easier to resolve as shown in Fig. 11(b). At this stage the island coverage decreased to 0.7 ML, although there was no noticeable increase in the pit density. Comparison of the filled and empty state images of the annealed surface in Figs. 11(c) and 11(d) suggests that the islands contain mostly Sb with bright spots in the empty state image attributed to Ge. Statistical analysis of these images suggests that 70% of the islands are Sb. The serpentine pattern of the islands can be understood in terms of the islands avoiding regions where Sb incorporated into the original surface layer. This ensures that all the lower surface energy Sb remains exposed.

Increasing the annealing temperature to 620 K induced further morphological changes to the surface. As shown in Fig. 11(e), the island coverage increased to 0.85 ML, the islands became larger and more compact, and new small islands started to grow on top of the islands that coalesced at 520 K. As a result, four layers are now exposed. This trend continued as the annealing temperature was increased. As shown in Fig. 11(f), at 800 K the surface is severely roughened with five layers exposed. The ISS data presented in Sec. III C indicate that annealing to these temperatures considerably increases the amount of Ge exposed in the surface layers. Although the surface roughens at 800 K, almost all the domain boundaries observed at lower temperatures are eliminated and thus the (2×1) LEED pattern sharpens.

When 3 ML of Sb were deposited at 320 K, no atomic resolution images could be obtained with STM prior to annealing. In this case the coverage was estimated from the AES peak intensity. In STM images, the surface appeared disordered with many large bumps. The disordered surface is consistent with LEED data that gave only a faint (1×1) pattern. Obtaining an ordered surface required desorbing the physisorbed Sb by annealing the sample past 600 K. Figures 12(a) and 12(b) show STM images taken after annealing at 620 K; AES spectra (not shown here) recorded at this stage indicate a nominal Sb coverage close to 1 ML. The images show a relatively smooth surface covered with symmetric dimers that are separated by many antiphase domain boundaries as highlighted by the arrows in Fig. 12(b). As a result of the domain boundaries, single atom wide vacancy strips are left on the surface that are too narrow to accommodate Sb dimers. In addition to the vacancies that result from the domain boundaries, wider vacancy islands and short strands of ad-dimers can also be seen in the images in Figs. 12(a) and 12(b); the coverage of these features is 0.05 ML and 0.08 ML, respectively.

Dual bias imaging of the surface prepared by annealing 3 ML of Sb at 620 K gave interesting contrast variations in empty state images as shown in Figs. 12(c) and 12(d). In the empty state image, the ad-dimers were difficult to detect suggesting that they are chemically different from the terrace. If this is again taken as an indication that the ad-dimers are Sb, it suggests that the surface is predominantly covered by Ge dimers. Both ISS [Fig. 3(c)] and AES, however, indicate that the surface is predominately covered by Sb. Also, the lack of any buckled dimers argues against a Ge-terminated surface. Alternatively, it can be argued that the contrast in this case is due to Sb in different chemical environments. One possibility is that the ad-dimers are second layer Sb dimers residing on top of the Sb layer bound to the Ge surface. In this case the difference in chemical bonding between the ad-dimers and the terraces would be the source of the contrast. This appears unlikely, however, because at 620 K any second layer Sb would be rapidly sublimed. Further, annealing at higher temperatures did not remove the ad-dimer islands but rather increased their size and coverage. By 800 K, the surface was severely roughened as shown in Fig. 12(e). Alter-

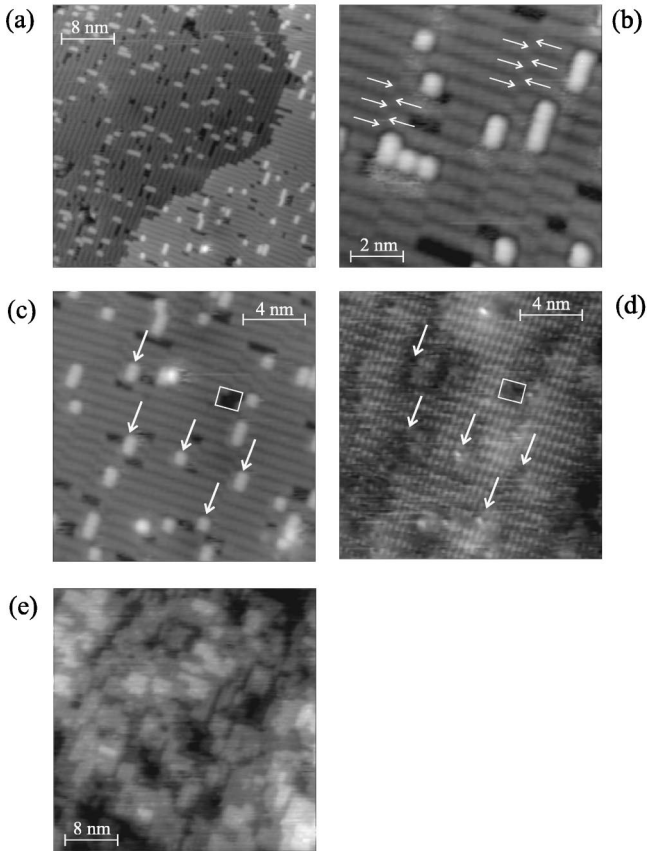

FIG. 12. Images of 3 ML Sb deposited at 320 K and then annealed at 620 K (a)–(d) and 800 K (e). A representative image of the surface morphology (a) after annealing shows many small islands and pits on the surface. A higher resolution image (b) shows that the dimers are separated by many antiphase domain boundaries indicated by the arrows. All the islands and some patches of the layer below appear dark in empty state image (d) while they have the same apparent height in the corresponding filled state image (c). The arrows highlight the same location on the surface in (c) and (d); the box highlights a pit that appears nonuniform in (d). $V_s = -1.25$ V for all images except (d) (1.25 V).

natively, the ad-dimers in Figs. 12(a)–12(c) could be Sb dimers on top of small Ge islands that form as a result of Sb incorporation into the original surface layer in the wider pits. The contrast in the pit highlighted in Figs. 12(c) and 12(d) as well as the low energy shoulder in the ISS spectrum in Fig. 3(c) support this assignment. Differences in chemical bonding in very small clusters and at step edges would then account for the decrease in apparent height of the ad-dimers in empty state images.

To see if kinetic limitations play a role in determining the morphology observed after annealing multilayer Sb films at 620 K, the surface morphology was also characterized following Sb deposition at elevated temperatures. Figure 13 shows a STM image obtained after exposing the Ge surface to an Sb fluence of 3 ML; the fluence was estimated from Sb deposition rates calculated from STM and AES data recorded at lower substrate temperatures. Auger spectra recorded after deposition (not shown here) indicate that only 1 ML of Sb remains on the surface. The ISS spectrum shown

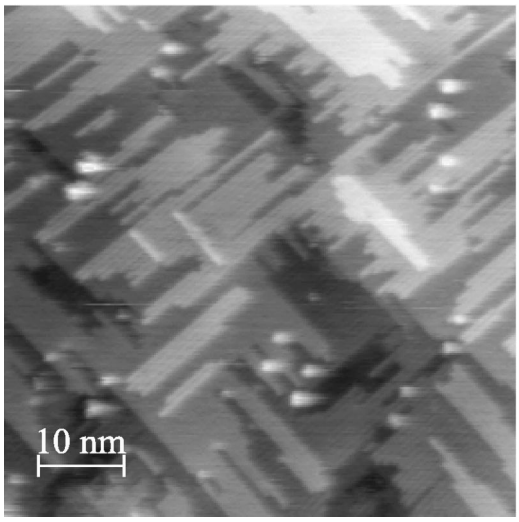

FIG. 13. Scanning tunneling micrograph of a surface prepared by exposing a fluence of 3 ML of Sb to Ge(100) above 600 K. $V_s = -1.00$ V and $I_t = 0.5$ nA.

in Fig. 3(e) also suggests that the surface is covered predominantly with Sb. Figure 13 shows that deposition at temperatures where Sb and Ge can exchange produces a surface with long, narrow islands, criss-crossing many exposed layers. In general, we find that depositing at elevated temperatures leads to much rougher surfaces than deposition at 320 K followed by annealing to the same temperature. This indicates that covering the surface with Sb at low temperatures creates kinetic roadblocks to Sb-induced surface roughening.

IV. DISCUSSION

The results provide the following detailed picture of Sb growth on Ge(100). The Sb arrives at the surface as Sb_4 clusters and initially adsorbs as intact, three-dimensional tetramers. These ball-shaped tetramers convert to square, flat tetramers through an activated process. The flat tetramers can split either parallel or perpendicular to the substrate dimer rows to form pairs of Sb dimers; the splitting is reversible. The perpendicular orientation is favored since this represents the epitaxial position. Perpendicular Sb dimers lie centered along the Ge dimer rows. This places the dimer directly above the dangling bonds of four nondimerized Ge atoms, suggesting that Sb lifts the Ge surface reconstruction, even at room temperature. Both Sb dimers and square, flat tetramers migrate across the surface. The flat tetramers can diffuse on the surface in two ways. The intact tetramer can hop one lattice spacing perpendicular to the substrate dimer rows. In addition, the tetramer can split into a pair of Sb dimers atop adjacent substrate dimer rows, and then reform when one of the dimers moves to the trough position adjacent to the other dimer; the resulting tetramer is shifted one lattice constant perpendicular to the substrate dimer rows. Below 520 K, Sb remains on top of the surface and the diffusion of tetramers and dimers leads to the formation of strings of Sb dimers. The shape of the resulting (2×1) domains is highly anisotropic, with the length in the $1\times$ direction much greater than that in the $2\times$ direction. This leads to an apparent (1×1)

LEED pattern at 1 ML at low energies. In prior experimental studies of Sb on Si(100) using reflectance anisotropy spectroscopy, angle resolved ultraviolet photoelectron spectroscopy, and LEED, a (1×1) phase was reported below 570–820 K.[41,42] Theoretical studies have also suggested a (1×1) Sb phase on Ge(100).[43] The STM results presented here, however, unequivocally show that Sb prefers to form dimers on the surface, and that even at low temperatures it forms a (2×1) structure on Ge(100).

Above 520 K, the diffusing Sb species can exchange places with Ge atoms in the surface layer. For each Sb dimer incorporated into the substrate, more than one Ge dimer is ejected, leading to pitting. The liberated Ge atoms migrate across the surface and either attach to preexisting steps or nucleate islands. The pit and island formation roughens the surface; where we started with one layer exposed, now at least three layers are exposed. As the Sb deposition is continued, migrating Sb is incorporated into the islands by both attachment to the island edges and exchange with Ge in the island interior; the liberated Ge can nucleate islands on top of the previously formed islands. Similarly, Sb-Ge exchange occurs within the pits, eventually causing pits to form within pits. The resulting roughened surface contains both Sb and Ge in every exposed layer. Increasing the Sb coverage toward 1 ML causes further changes in the surface morphology. Because Sb has a lower surface tension than Ge, and because the Sb-Ge interaction is much stronger than the Sb-Sb interaction, Sb prefers to be exposed, positioned on top of Ge. At high coverages, however, Sb-Ge intermixing is not possible without burying Sb beneath either Sb or Ge. Increasing the surface area by further roughening allows Sb-Ge intermixing without burying Sb beneath the surface. Ultimately, the surface roughness will be limited by the trade-off between the energy cost of increasing the surface area versus the energy gained by Sb-Ge surface intermixing.

The intermixing and associated roughening observed above 520 K can be limited by completely covering the Ge surface with Sb at lower temperatures and then annealing. At these coverages, simple Sb-Ge exchange cannot occur without at least briefly burying Sb beneath the surface and so a higher energy barrier to exchange is expected. Alternatively, complex, concerted exchange mechanisms that keep the Ge beneath the Sb can be envisioned, particularly at the numerous domain boundaries in the Sb layer; however, such mechanisms are also likely to have a much higher energy barrier than exchange of an isolated Sb dimer. Thus intermixing and roughening are kinetically limited by covering the surface with Sb at low temperatures. As a result, relatively well-ordered, smooth, Sb-terminated surfaces can be obtained by either carefully depositing 1.0 ML of Sb at room temperature and annealing to 520 K, or depositing Sb multilayers at room temperature and then annealing to 620 K to desorb all but the first layer. Raising the annealing temperature to 800 K, however, is sufficient to overcome the barrier to Sb-Ge exchange in a complete Sb monolayer and the surface roughens with intermixed Sb-Ge islands exposed on multiple layers. Thus as the annealing temperature is increased surfaces prepared by covering the surface with Sb at low temperatures and then annealing become essentially indistinguishable from those prepared by depositing Sb at high temperature. A consequence of this is that TPD could not be used to determine energy differences between on-top and in-surface Sb, since at the high desorption temperatures surface intermixing always occurs, regardless of how the surface is prepared.

The results indicate that surface intermixing plays a key role in determining the morphology of Sb-covered Ge surfaces. In recent years, surface intermixing has been observed for a number of systems that, like Sb and Ge, are essentially immiscible in the bulk. These include Rh on Au,[44] Ni on Ag(111),[45] Fe on Cu(100),[46] Au on Ni(110),[47] and As on Si(100).[48] For Au on Ni(110), lower surface tension, larger Au atoms displace Ni atoms in the surface. Nielsen *et al.*[47] suggested that Au-Ni exchange is driven by the larger, more electron-rich Au atoms increasing the effective coordination of the neighboring Ni atoms in the surface toward their bulk value. Phrased another way, the reduced coordination of the Ni atoms on the surface creates tensile stress that can be relieved by substituting larger Au atoms into the surface. Antimony is 16% larger than Ge and, like Au and Ni, has one more electron than Ge and so similar arguments can be invoked to explain the driving force for Sb-Ge exchange. A difference between the Sb-Ge(100) system and the other systems where surface intermixing has been observed is that intermixing is accompanied by pitting. The pitting can be explained in terms of the (2×1) reconstruction creating compressive stress parallel to the dimer rows (the $2\times$ direction), while the stress remains tensile perpendicular to the dimer rows (the $1\times$ direction).[49] Thus Sb substitution relieves stress in the Ge surface in one direction, but exacerbates it in the other. The pitting can relieve the stress. Again, the energy gained by stress relief must exceed the cost of the added step energy due to the islands and pits. The long, narrow pits oriented perpendicular to the $2\times$ direction can be understood in terms of reducing the step energy since steps running parallel to the dimer rows on the upper terrace are lower in energy.[50]

Regardless of the driving force for intermixing, exchange has important implications for surfactant-mediated thin film growth. It is apparent that this process can lead to the surfactant severely roughening the surface, even for a simple, single component system. As a result, the surfactant coverage and the growth temperature must be carefully controlled or addition of the surfactant will actually roughen the surface. For Sb-mediated Ag(111) homoepitaxy, it has been shown that a $(\sqrt{3}\times\sqrt{3})R30°$ Sb-Ag alloy layer acts as the surfactant layer during growth.[9] If the Sb coverage is higher than 1/3 of a monolayer, not all the Sb can exchange to form the alloy surface, since this would dictate at least partially covering the lower surface energy Sb with either Ag or Sb. Thus an Sb coverage beyond 1/3 of a monolayer can be detrimental to the process. Unlike Sb on Ag, however, no ordered Sb-Ge surface alloys were observed other than Sb forming patches within the Ge surface. As a result, a maximum Sb coverage is less obvious in this case, although it is clear that for high growth temperatures the substitutional Sb coverage should be much less than 1 ML.

The results described here for the single component sys-

tem raise interesting questions about using surfactant-mediated heteroepitaxy. The most commercially important system using surfactant-mediated growth is Sb-mediated Ge growth on Si(100).[1] It has now been established that Sb intermixes with Si(100) (Ref. 20) and Ge(100) surfaces, and in both cases this can be rationalized in terms of relieving tensile surface stress. Germanium is larger than Si and so epitaxial Ge is compressed. One might expect this compression to remove the driving force for Sb exchange into the Ge layer. Conversely, Si layers on Ge(100) would be under tensile stress and so we would expect even more extensive Sb intermixing in this case. At present, it is not known if Sb also intermixes with thin, epitaxial Ge layers on Si(100) or Si layers on Ge(100). If intermixing occurs during Sb-mediated Ge growth on Si(100), the potential for surface roughening should be even greater than for Ge homoepitaxy. Since the Ge is already compressed on the Si surface, Sb exchange would be accompanied by more extensive pitting and islanding than on a Ge substrate in order to relieve the greater stresses. Thus the surfactant coverage is also expected to play a key role in surfactant-mediated heteroepitaxy.

V. SUMMARY

The interaction of Sb with the Ge(100) surface has been studied as a function of Sb coverage and annealing temperature. At 320 K, antimony initially adsorbs on Ge(100) as a three-dimensional (3D) cluster. The 3D clusters can convert to flat tetramers that can then split into pairs of dimers. The splitting of the tetramer is reversible at room temperature. The tetramers diffuse both by splitting and reforming at a position shifted by one lattice constant, and by hopping as an intact unit. The dimers also diffuse, and collisions of tetramers and dimers lead to strings of Sb dimers separated by antiphase domain boundaries that characterize Sb growth on Ge(100) at 320 K. Intermixing of Sb with Ge starts at 520 K for low Sb coverages. The incorporation of Sb into the surface layer displaces Ge that then diffuses on the surface. The liberated Ge roughens the existing step edges and creates pits on the surface. As the Sb coverage increases to 0.4 ML, after annealing at 520 K both pits and islands are created leaving all exposed layers intermixed with Sb and Ge. A relatively smooth Sb overlayer can be prepared by covering the surface with nearly 1 ML Sb and annealing at 520 K. Under these conditions, intermixing is limited by the lower surface tension of Sb which dictates that all the Sb must be exposed on the surface. An alternative method to prepare a smooth Sb overlayer is to deposit more than 1 ML Sb, and then anneal to 620 K to desorb all physisorbed Sb. Subsequent annealing at higher temperature severely roughens the surface, independent of how the Sb layer is prepared. The intermixing can be understood as a result of relieving surface stresses at the expense of increasing the surface area. Therefore, it is critical to carefully control the growth of the surfactant layer because intermixing can roughen the film rather than promoting layer-by-layer growth during surfactant-mediated growth.

ACKNOWLEDGMENTS

The authors acknowledge the assistance of Guowen Zheng, Robert Tanner, and Min Li in carrying out this work. This project was supported by the National Science Foundation under Grant No. CTS-9733416.

[1] M. Copel, M. C. Reuter, E. Kaxiras, and R. M. Tromp, Phys. Rev. Lett. **63**, 632 (1989).
[2] H. A. van der Vegt, H. M. van Pinxteren, M. Lohmeier, E. Vlieg, and J. M. C. Thornton, Phys. Rev. Lett. **68**, 3335 (1992).
[3] K. H. Park, J. S. Ha, S. J. Park, and E. H. Lee, Surf. Sci. **380**, 258 (1997).
[4] J. Vrijmoeth, H. A. van der Vegt, J. A. Meyer, E. Vlieg, and R. J. Behm, Phys. Rev. Lett. **72**, 3843 (1994).
[5] B. Voigtländer and A. Zinner, J. Vac. Sci. Technol. A **12**, 1932 (1994).
[6] B. Voigtländer, A. Zinner, T. Weber, and H. P. Bonzel, Phys. Rev. B **51**, 7583 (1995).
[7] J. A. Meyer, J. Vrijmoeth, H. A. van der Vegt, E. Vlieg, and R. J. Behm, Phys. Rev. B **51**, 14 790 (1995).
[8] J. A. Meyer, H. A. van der Vegt, J. Vrijmoeth, E. Vlieg, and R. J. Behm, Surf. Sci. **355**, L375 (1996).
[9] T. C. Q. Noakes, D. A. Hutt, C. F. McConville, and D. P. Woodruff, Surf. Sci. **372**, 117 (1997).
[10] D. H. Rich, T. Miller, and T.-C. Chiang, Phys. Rev. B **41**, 3004 (1990).
[11] G. Falkenberg, L. Seehofer, and R. L. Johnson, Surf. Sci. **377**, 75 (1997).
[12] D. H. Rich, F. M. Leibsle, A. Samsavar, E. S. Hirschorn, T. Miller, and T.-C. Chiang, Phys. Rev. B **39**, 12 758 (1989).
[13] D. H. Rich, T. Miller, G. E. Franklin, and T.-C. Chiang, Phys. Rev. B **39**, 1438 (1989).
[14] D. H. Rich, G. E. Franklin, F. M. Leibsle, T. Miller, and T.-C. Chiang, Phys. Rev. B **40**, 11 804 (1989).
[15] A. Lessmann, W. Drube, and G. Materlik, Surf. Sci. **323**, 109 (1995).
[16] M. Lohmeier, H. A. van der Vegt, R. G. van Silfhout, E. Vlieg, J. M. C. Thornton, J. E. Macdonald, and P. M. L. O. Scholte, Surf. Sci. **275**, 190 (1992).
[17] M. Richter *et al.*, Phys. Rev. Lett. **65**, 3417 (1990).
[18] J. Nogami, A. A. Baski, and C. F. Quate, Appl. Phys. Lett. **65**, 475 (1991).
[19] H. B. Elswijk and E. J. v. Loenen, Ultramicroscopy **42-44**, 884 (1992).
[20] B. Garni, I. L. Kravchenko, and C. T. Salling, Surf. Sci. **423**, 43 (1999).
[21] Y. W. Mo, Phys. Rev. Lett. **69**, 3643 (1992).
[22] Y. W. Mo, Phys. Rev. B **48**, 17 233 (1993).
[23] Y. W. Mo, Phys. Rev. Lett. **71**, 2923 (1993).
[24] Y. W. Mo, J. Vac. Sci. Technol. B **12**, 2231 (1994).
[25] M. A. Boshart, A. A. Bailes III, A. Dygo, and L. E. Seiberling, J. Vac. Sci. Technol. A **13**, 2764 (1995).

[26] C. Y. Nakakura, V. M. Phanse, G. Zheng, G. Bannon, E. I. Altman, and K. P. Lee, Rev. Sci. Instrum. **69**, 3251 (1998).
[27] K. D. John, K. J. Wan, and J. T. Yates, Jr., J. Vac. Sci. Technol. B **11**, 2137 (1993).
[28] L. H. Chan, E. I. Altman, and Y. Liang, J. Vac. Sci. Technol. A (to be published).
[29] R. Hultgren, R. L. Orr, P. D. Anderson, and K. K. Kelly, *Selected Values of Thermodynamic Properties of Elements* (Wiley, New York, 1973), p. 448.
[30] R. W. Olesinski and G. J. Abbaschian, Bull. Alloy Phase Diagrams **7**, 219 (1986).
[31] A. D. Johnson, C. Norris, J. W. M. Frenken, H. S. Derbyshire, J. E. MacDonald, R. G. van Silfhout, and J. F. van der Veen, Phys. Rev. B **44**, 1134 (1991).
[32] Energy is approximated by $n_{B1}/n_{B2}=K=e^{-\Delta G/kT}$, where K is the equilibrium constant, n the concentration, k Boltzmann's constant, and T temperature.
[33] X. R. Qin and M. G. Lagally, Science **278**, 1444 (1997).
[34] R. J. Hamers, U. K. Kohler, and J. E. Demuth, J. Vac. Sci. Technol. A **8**, 195 (1990).
[35] Y. Wang, M. J. Bronikowski, and R. J. Hamers, J. Vac. Sci. Technol. A **12**, 2051 (1994).
[36] H. J. W. Zandvliet, B. S. Swartzentruber, W. Wulfhekel, B. J. Hattink, and B. Poelsema, Phys. Rev. B **57**, R6803 (1998).
[37] E. J. Kirchner, Ph.D. thesis, University of Amsterdam, 1994.
[38] R. J. Culbertson, Y. Kuk, and L. C. Feldman, Surf. Sci. **167**, 127 (1986).
[39] R. Rossmann, H. L. Meyerheim, V. Jahns, J. Wever, W. Moritz, D. Wolf, D. Dornisch, and H. Schulz, Surf. Sci. **279**, 199 (1992).
[40] R. M. Tromp, Phys. Rev. B **47**, 7125 (1993).
[41] A. Cricenti, S. Selci, A. C. Felici, L. Ferrari, G. Contini, and G. Chiarotti, Phys. Rev. B **47**, 15 745 (1993).
[42] J. R. Power, T. Farrell, P. Gerber, S. Chandola, P. Weightman, and J. F. McGilp, Surf. Sci. **372**, 83 (1997).
[43] R. H. Miwa, Appl. Surf. Sci. **142**, 52 (1999).
[44] E. I. Altman and R. J. Colton, Surf. Sci. **304**, L400 (1994).
[45] F. Maroun, S. Morin, A. Lachenwitzer, O. M. Magnussen, and R. J. Behm, Surf. Sci. **460**, 249 (2000).
[46] D. D. Chambliss and K. E. Johnson, Phys. Rev. B **50**, 5012 (1994).
[47] L. P. Nielsen, F. Besenbacher, I. Stensgaard, E. Laegsgaard, C. Engdahl, P. Stoltze, K. W. Jacobsen, and J. K. Norskov, Phys. Rev. Lett. **71**, 754 (1993).
[48] R. M. Tromp, A. W. Denier van der Gon, and M. C. Reuter, Phys. Rev. Lett. **68**, 2313 (1992).
[49] R. D. Meade and D. Vanderbilt, in *Twentieth International Conference on the Physics of Semiconductors*, edited by E. M. Anastassakis and J. D. Joannopoulos (World Scientific, Singapore, 1990), p. 123.
[50] D. J. Chadi, Phys. Rev. Lett. **59**, 1691 (1987).